Journal Pre-proof

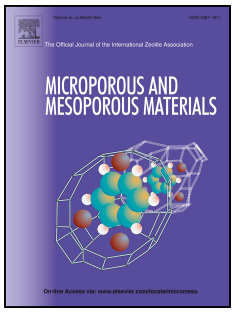

Water viscosity in confined nanoporous media and flow through nanofiltration membranes

Sara Álvarez-Quintana, Francisco Javier Carmona, Laura Palacio, Antonio Hernández, Pedro Prádanos

PII: S1387-1811(20)30292-4

DOI: https://doi.org/10.1016/j.micromeso.2020.110289

Reference: MICMAT 110289

To appear in: *Microporous and Mesoporous Materials*

Received Date: 24 February 2020

Revised Date: 12 April 2020

Accepted Date: 22 April 2020

Please cite this article as: S. Álvarez-Quintana, F.J. Carmona, L. Palacio, A. Hernández, P. Prádanos, Water viscosity in confined nanoporous media and flow through nanofiltration membranes, *Microporous and Mesoporous Materials* (2020), doi: https://doi.org/10.1016/j.micromeso.2020.110289.

CRediT author statement

Sara ÁLVAREZ-QUINTANA: Investigation. **Francisco Javier CARMONA:** Investigation, Validation Verification. **Laura PALACIO:** Investigation, Formal analysis, Funding acquisition. **Antonio HERNÁNDEZ*:*** Supervision. Writing - Review & Editing. **Pedro PRÁDANOS:** Conceptualization, Methodology, Supervision, Writing - Original Draf, Writing - Review & Editing**.**

Water viscosity in confined nanopores and temperature

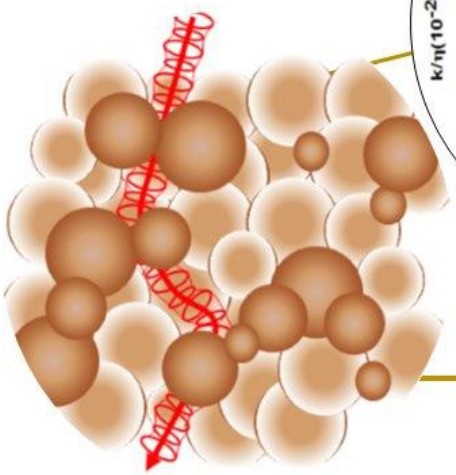

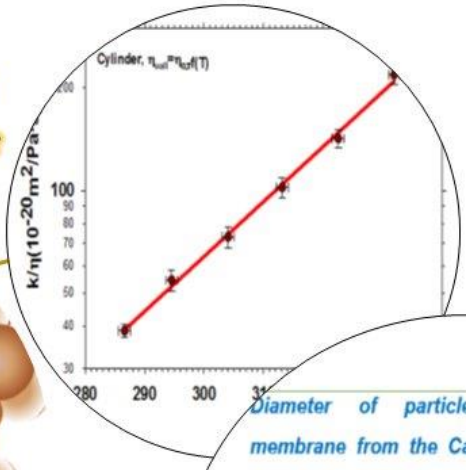

Diameter of particles forming the membrane from the Carman-Kozeny and our model for the membrane In09nm. The percentages of deviation from the particle size as measured by AFM are also shown.

Model	$D_p(nm)$	$\frac{D_p - D_{p,AFM}}{D_{p,AFM}}100$ (%)
Cylindrical pores $\eta_{wall} = \eta_{0,T} f(T)$	7.42 $\pm$ 0.2	-5.7

Water viscosity in confined nanoporous media and flow through nanofiltration membranes.

Sara ÁLVAREZ-QUINTANA[1], Francisco Javier CARMONA[2], Laura PALACIO[1], Antonio HERNÁNDEZ[1], Pedro PRÁDANOS[1].*

[1]*Grupo de Superficies y Materiales Porosos, Dpto. Física Aplicada, Facultad de Ciencias, Universidad de Valladolid, 47071, Valladolid, Spain.*

[2]*Dpto. Física Aplicada. Escuela Politécnica, Universidad de Extremadura, 10004 Cáceres, Spain*

***Corresponding Author:** *E-mail: pradanos@termo.uva.es*

Abstract

Nanofiltration flux and selectivity depend on the mass transfer through the nanometric pores. Among other factors, including charges and dielectric constant for the charged species, viscosity is of crucial relevance. Here we study how viscosity changes in confined media in the nanometric range. The models found in the literature, that assume that the ratio of the viscosity of water on the pore walls over that in bulk water is a constant, are totally unsatisfactory to predict the dependence of the Darcy constant on temperature.

Pure water flux is studied as a function of temperature for three commercial ceramic membranes. For these membranes, we fit flow versus temperature with a quite good fitting assuming that the first layer of water on the cylindrical pore walls move with a viscosity $\eta_p = \eta_0 A e^{-\frac{E_a}{RT}}$. If the flow is assumed to follow a Carman-Kozeny equation, according to its more realistic granular nature, the resulting porosity and mean grain size are in accordance with the data known and measured by atomic force microscopy (AFM).

Keywords: Nanoconfined water, Water viscosity, Water adsorption energy, Nanofiltration, Ceramic membranes.

1. Introduction

Nanofiltration [1] retains non-ionic molecules in the range from 100 to 1000 g/mol, i.r. with radii around 1 nm. It is also intensively used to reject divalent ions for water descaling and de-sulphating. Some retention of monovalent ions appears too, including sodium, potassium, bicarbonates, nitrates etc. Of course, in nanofiltration the retentions of mono-valent ions are lower than in reverse osmosis, but it operates at lower pressures.

Actually, osmotic, but also diffusive, electric and dielectric effects must be taken into account when analyzing the transport through nanofiltration membranes [2, 3]. Many models have been tested to explain the transport of ionic and non-ionic species through nanofiltration membranes [4]. By now, it has become evident that an adequate knowledge of: size, length and density of pores in the active layer would be needed to model nanofiltration flux and selectivity. Other factors of interest concerning the pores in a nanofiltration membrane include their electric and dielectric characteristics.

The simplest model refers to the flux inside a cylindrical pore. As known, it presents a parabolic velocity profile in laminar conditions that after integration allows us to correlate the volume flow caused by a gradient of pressure according to the Hagen-Poiseuille equation [5]. Another equation, used for the volume flow in terms of the pressure gradient, is due to Carman and Kozeny. This model is especially fitted to study the flow through non uniform media defining channels or pores along paths in random directions which is very appropriate for sandy or fibrous media that are usually modeled as consisting in a packing of differently sized particles [6].

In order to model the movement of a liquid or solution inside the pores, a good knowledge of the physical properties of the fluid is crucial. For example, density, viscosity and dielectric constant would be required. But actually, all these properties can vary significatively when the liquid is confined within nanometric pores [7]. The dielectric constant has been evaluated by using impedance spectroscopy proving that it decreases as an effect of confinement [8]. Here we will focus on the viscosity of pure water without any ion in presence to isolate its effects from the electric or dielectric ones.

Some authors consider that, for nanopores, all fluids should be supposed as discrete phases rather than continuous matter. Nevertheless, it is generally accepted in literature that the classical fluid mechanics laws can describe the fluid, even within nanometer scale dimensions, with small "ad hoc" corrections. For example, Bowen and Welfoot [2] used the Hagen-Poiseuille equation to describe the velocity of liquids through nanoporous membranes, but they assumed a thin layer on the pore walls with a higher viscosity.

Others [9, 10] went a little further and considered that the non-slipping condition on the pore walls, which is typically admitted, should be reconsidered for systems with a high surface/volume ratio, [9]. Then, the Navier-Stokes equation should be integrated with other more appropriate boundary conditions without any non-slipping layer at the pore walls because fluid-wall interactions are intense but not infinite. The slipping conditions on the pore walls would be substituted by a zero tangential speed on an extrapolated virtual surface placed somewhere inside the pore material at a so called slipping length from the actual pore walls [11, 12]. This slipping length can be given as a function of the solvent-membrane interactions [13] but models that assume different slipping lengths have been tested for inorganic nanofiltration and ultrafiltration membranes and a broad range of pure and mixed liquids [13] without general conclusions. In all cases, the corresponding integrations would give modified Hagen-Poiseuille equations.

Anyway, it seems clear that, the Hagen-Poiseuille equation might be corrected. We will assume here that the permeate volume flow per unit of area is $J_V = J_{V,HP}\left(1+f_C\right)$ with $J_{V,HP}$ the Hagen-Poiseuille flux. Usually f_C is taken as a function of δ/r_p (δ is the slipping length and r_p is the pore radius) determined by the interactions between water and membrane. Here, we will assume $f_C\left(d/r_p\right)$ with d being the thickness of the first layer of adsorbed water. This first layer can be assumed to slip on the pore walls as a rigid body with a viscosity which is proportional to the bulk one. These assumptions follow and generalize the lines proposed by Bowen and Welfoot [2]. The existence of adsorbed low-mobility layers of water has been demonstrated on the surfaces of hydrophilic porous metal oxides. For example, González Solveyra et al [14] and Velasco et al [15] have modelled and measured these layers by NMR Relaxometry.

In our case, d corresponds to an adsorbed water layer whose interaction has been modelled as a function of temperature according to an Arrhenius dependence. Note that δ depends on the interaction but the details of this interaction and its dependence on temperature are mostly unknown.

From a methodological point of view, we will measure the volume flow of pure water through nanofiltration membranes at different temperatures. By modelling the dependence of water-membrane interaction on temperature by an Arrhenius' equation we will find the radial dependence of viscosity inside the pores in conditions of relevant confinement for different temperatures.

2. Theory

2.1. Flux equations

The Darcy's law gives the volume flow, J_V, per unit area through a porous material as proportional to the pressure gradient $J_V = K\left(\Delta p / l_m\right)$ with K being the Darcy constant, Δp the pressure drop and l_m the thickness of the membrane. It is worth noting that when dealing with asymmetric, supported or composite membranes, l_m, is the thickness of the active layer. The presence of a supporting structure is required to give mechanical stability without affecting significantly flow and retention.

If we include viscosity, η, explicitly [16]:

$$J_V = \frac{k}{\eta}\frac{\Delta p}{l_m} \tag{1}$$

with k a multiplicative constant ($k = K\eta$) that should depend only on the geometric properties of the porous membrane.

In order to get explicit expressions for k, a detailed model needs to be assumed. For example, if the membrane consists in a bunch of cylindrical pores that are perpendicular to both the membrane surfaces, the Navier-Stokes equation can be solved, with the non-slipping condition on the walls and incompressible and stationary flow, to get the well-known Hagen-Poiseuille equation:

$$J_V = \frac{\pi n_p \Delta p}{8\eta l_m} r_p^{\,4} = \frac{\varepsilon \Delta p}{8\eta l_m} r_p^{\,2} \tag{2}$$

n_p is the number of pores per unit of area and ε is the surface porosity (which, for parallel pores perpendicular to the membrane surface), is the volume porosity [17]:

$$\varepsilon = \frac{A_\varepsilon}{A_m} = \pi n_p r_p^{\,2} \tag{3}$$

A_ε is the membrane area opened to flow, whereas A_m is the total transversal area of the membrane. If pores are not parallel to each other or are not perpendicular to the membrane surfaces, a tortuosity factor can be defined:

$$\tau = \frac{l}{l_m} \tag{4}$$

being l the length of the pores. In this case, Eq. (2) can be rewritten as:

$$J_V = \frac{\varepsilon \Delta p}{8\eta \tau l_m} r_p^2 \tag{5}$$

and:

$$k = \frac{\varepsilon}{8\tau} r_p^{\,2} = \frac{\pi n_p}{8\tau} r_p^{\,4} \tag{6}$$

It is worth noting that in fact there is a pore size distribution thus r_p in Eqs. (2), (3), (5) and (6) must be interpreted as an average representative pore radius [2, 18]. The use of pore size distributions would require a technique allowing the elucidation of these pore size distributions on nanofiltration membranes, which is not a simple question, leading to unnecessary complications of the model.

If slit-like pores ($H \times h$ rectangles with $H \gg h$) are considered, Eq. (2) must be substituted (without taking into account any border effects along h) by:

$$J_V = \frac{\varepsilon \Delta p}{12\eta \tau l_m} h^2 \tag{7}$$

and:

$$k = \frac{\varepsilon}{12\tau} h^2 \tag{8}$$

It has become customary, mainly for inorganic membranes, to assume porous materials as formed by differently sized and more or less closely packed spheres. The

fluid would follow complicated paths as shown in Fig. 1 Then, flux is somehow similar to that through capillary pores [6]. In these cases, assuming an equivalent hydrodynamic pore radius as twice the cross-section area divided by the wet perimeter:

$$J_V = \frac{\varepsilon^3 D_{part}^2 \Delta p}{72\eta(1-\varepsilon)^2 \tau l_m} \tag{9}$$

D_{part} is the average particle diameter within the active layer of the membrane. Moreover, here ε is the volume porosity that would differ from the surface one. Some theoretical and phenomenological considerations for such porous systems concluded that, in these cases, $\tau = 2.5$ [6]. Thus leading to the Carman-Kozeny equation which is equivalent to Eq. (1) with:

$$k = \frac{\varepsilon^3 D_{part}^2}{180(1-\varepsilon)^2} \tag{10}$$

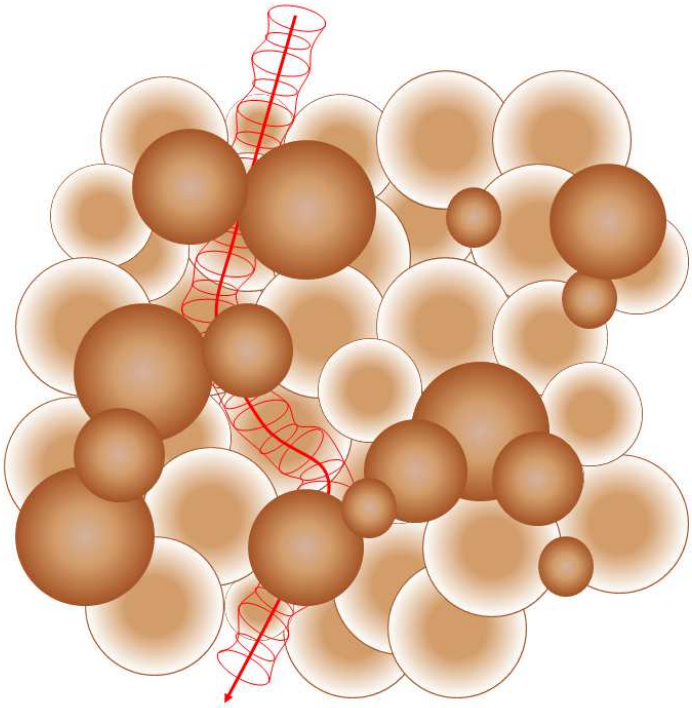

Fig. 1.- A channel made out of interstices between a particulate material.

2.2. Viscosity in nanopores

When dealing with pores of sizes of the same order than the size of the molecules of the fluid transported through them, the consideration of the fluid as a continuum is compromised. Some natural corrections are aimed to consider viscosity as radius depending magnitude more or less different from its bulk value. One of the first proposals in this direction was made by Bowen and Welfoot [2]. They considered that there is a first adsorbed layer of water in contact with the pore walls characterized by a viscosity 10 times bigger than the bulk one, which is also characterizing the flux outside that adsorbed layer. Afterwards they averaged viscosity on the total cross section of the pore to get:

$$\frac{\eta_p}{\eta_o} = 1 + 18\left(\frac{d}{r_p}\right) - 9\left(\frac{d}{r_p}\right)^2 \tag{11}$$

Here d is the thickness of the adsorbed water molecules and can be assumed to be d = 0.28 nm as already made clear by Bowen and Welfoot [2], r_p is the pore radius and η_o the bulk viscosity.

For a Hagen-Poiseuille flow the volume flow (through the total porous area, $Q_V = J_V A_m$) is:

$$Q_V \propto \frac{r_p^4}{\eta_p} \tag{12}$$

Then, the corresponding average (or equivalent total) viscosity can be obtained from Q_V versus r_p experiments, as Wesolowskaa et al. did for cylindrical pores [7], to give:

$$\eta_p = \left[(1-y)^4/\eta_0 + y\left(4 - 6y + 4y^2 - y^3\right)/(10\eta_0)\right]^{-1} \tag{13}$$

with $y = d/r_p$.

If the pores are assumed to be slit shaped, by the same procedure used by Wesolowskaa et al. [4], viscosity is:

$$\eta_{p,slit} = \frac{10\eta_0}{1 + 9\left(1 - d/r_{p,slit}\right)^3} \tag{14}$$

with $r_{p,slit} = h/2$.

To get Eqs. (13) and (14), $\eta_{wall} = 10\eta_0$ must be assumed, like Bowen and Welfoot [2] did to get Eq. (11).

In Fig. 2 the dependence of the viscosity ratio (η_p/η_0) is shown versus pore radius, r_p, for the three models mentioned so far. Bowen and Welfoot [2] predict $\eta_p/\eta_0 > 2$ or higher for pores up to about 5 nm. Viscosity is higher for cylindrical pores which seems logical because there is more confinement within cylindrical pores than inside slit-like ones. In Fig. 2 it can be seen that only for $r_p > 20$ nm, Eqs. (13) and (14) lead to $\eta_p/\eta_0 < 1.05$. This means that only for pore radii over 20 nm, viscosities η_p are less than 5 % above that of bulk (unconfined) water. Note that for pores with r_p = 0.5 nm the pore overall viscosity would be higher than 6 times the bulk water value for the three models.

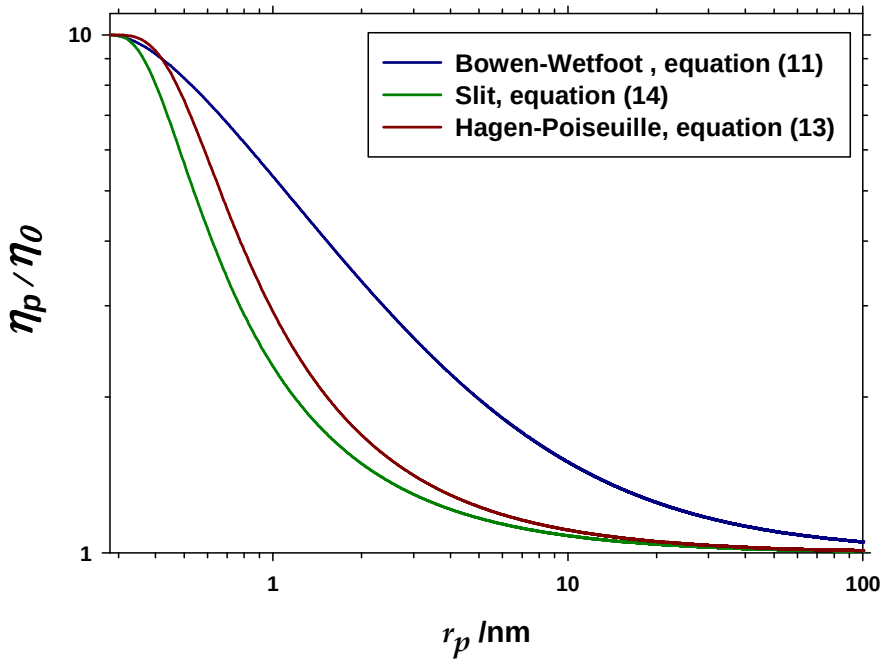

Fig. 2.- Viscosity as a function of pore size for the three models mentioned in the figure.

According to these models, the first adsorbed layer onto the pore walls must be assumed to move with a high viscosity, η_{wall}, with equal slipping velocity within the adsorbed layer of thickness d ($r_p - d \le r \le r_p$). This means that, when obtaining the

Hagen-Poiseuille equation, the boundary condition usually assumed (i.e. non-slipping on the walls) has to be reconsidered. In general, as mentioned in the introduction, the tangential speed, v, must be assumed to be zero only on an extrapolated virtual surface parallel to the pore walls, at a distance δ (slipping length) inside the pore material. Then, the transport equations and boundary conditions are [9, 10, 13, 19-21]:

$$\left.\begin{aligned} &\frac{dv}{dr}=0, && r=0 \\ &v(r)=-\delta\frac{dv}{dr}, && r=r_p \end{aligned}\right\} \tag{15}$$

These equations lead to a modified Hagen-Poiseuille equation:

$$J_V = J_{V,HP}\left(1+f_C\right) \tag{16}$$

Here $J_{V,HP}$ is the classical Hagen-Poiseuille equation and f_C is a function of δ/r_p and the slipping length δ would be a function of the interactions between water and membrane. In the literature, there is not any widely accepted theoretical expression for δ although it has been proved that it depends on the liquid and the membrane material. The nature of the liquid controls the thickness of the slipping layer and the membrane-liquid interaction energy [13]. All the relationships shown so far for η_p/η_0 here (Eqs. (11) (13) and (14)) can be written as:

$$\frac{1}{\eta_p}=\frac{1}{\eta_0}\varphi\left(\frac{d}{r_p}\right) \tag{17}$$

And thus, in accordance with Eq. (16):

$$f_C=\varphi\left(\frac{d}{r_p}\right)-1 \tag{18}$$

Some authors consider that f_C (and φ in Eq. 18) would depend on other factors as, for example, capillary forces or dipolar interactions [13, 21], which seems essentially

true. However, we will assume here that, capillary forces are only relevant at the pore entrances, while polar interactions will be included in a water-membrane activation energy. In this work, in order to get an expression for f_C (or φ) we propose to generalize the relationship suggested by Wesolowska et al. [7], (Eq. (13)), to avoid the arbitrary assumption of a layer of viscosity 10 times the bulk one on the pore walls. To do that, we consider the temperature dependence $\eta_{wall}/\eta_0 = f(T)$ as an Arrhenius one $f(T) = Ae^{-\frac{E_a}{RT}}$ [22]. This Arrhenius expression correlates the adsorption kinetics with an activation energy E_a that embodies water-wall interactions.

Thus Eq. (13) would be:

$$\frac{1}{\eta_p} = \left(\frac{(1-y)^4}{\eta_{0,T}} + \frac{y\left(4-6y+4y^2-y^3\right)}{f(T)\eta_{0,T}} \right) \tag{19}$$

$\eta_{0,T}$ being the bulk viscosity at temperature T. In the same way, Eq. (14) would be substituted by:

$$\frac{1}{\eta_{p,slit}} = \frac{1+9\left(1-d/r_{p,slit}\right)^3}{f(T)\eta_{0,T}} \tag{20}$$

According to Eqs (5) and (19), the Darcy's constant can be written as:

$$K = \frac{k}{\eta_p} = k\left(\frac{(1-y)^4}{\eta_{0,T}} + \frac{y\left(4-6y+4y^2-y^3\right)}{\eta_{0,T}Ae^{-\frac{E_a}{RT}}} \right) \tag{21}$$

for cylindrical pores. For slit-shaped pores, Eqs. (7) and (20), would be:

$$K = \frac{k}{\eta_p} = k\left(\frac{1+9\left(1-d/r_{p,slit}\right)^3}{\eta_{0,T}Ae^{-\frac{E_a}{RT}}} \right) \tag{22}$$

The experimental determination of the Darcy's constant as a function of temperature will allow testing the suggested models.

3. Material and methods

3.1. Materials and Chemicals

Three nanofiltration tubular membranes manufactured by Inopor (Inopor, Rauschert Distribution GmbH, Veilsdorf, Thuringia, Germany), named as Inopor® Nano, have been used here. According to the manufacturer, these membranes are made on a porous support of α-alumina (α-Al_2O_3), with increasing pore size and porosity from the inner to the outer surface [23]. On this porous support there is a layer of titania, TiO_2, acting as a selective or active layer. The manufacturer does not mention that the active layer contains ZrO_2 as will be shown below from elemental analysis by energy dispersive spectroscopy (EDS). These membranes have high thermal resistance, up to 110^oC, and resist thermal oscillations as high as 20 K/s [24]. They have an external diameter of 7 mm with a specific area of 0.0220 m^2/m. Some of the characteristics of Inopor membranes, as given by the manufacturers, are shown in Table 1.

Table 1: Characteristics of the original ceramic membranes as given by the manufacturers [25]. MWCO is the molecular weight cutoff or the mass of molecules that are retained over 90 %.

Membrane (abbreviation)	**Water permeability (10^{-11} m/s·Pa)**	**MWCO (g/mol)**	**Pore-diameter (nm)**	**Porosity (%)**
Inopor ® nano 1 nm (In1nm)	3.6-9.8	750	1.0	30-40
Inopor ® nano 0.9 nm (In09nm)	3.6-9.8	450	0.9	30-40 (30%) [26]
Inopor ® nano LC (InLC)*	2.5	200	-	30-40

** The manufacturers do not give the pore diameter for InLC and no value for this pore diameter could be found in the literature.*

These membranes are almost unaffected by swelling and thermal dilation. Moreover, their pore sizes are low enough as to reveal clear effects of confinement on water flow through them and not so small as to retain water.

3.2. Membrane Characterization

3.2.1. Atomic Force Microscopy (AFM)

AFM images have been obtained by using a Nanoscope Multimode IIIa® from Digital Instruments (Veeco Metrology Inc., Santa Barbara, California, USA) in the tapping mode in accordance to methods shown elsewhere [4]. Grain size, Roughness

and Power Spectral Density (PSD) have been analyzed by using the NanoScope Software Version 5.30.

3.2.2. Scannig Electron Microscopy (SEM) y Energy Dispersive Spectroscopy (EDS)

A SEM device FEI Quanta 200 FEG (FEI Company, Hillsboro, Oregon, USA) has been used to image the membrane surfaces and transversal cuts and to perform EDS analysis. To perform elemental analysis, the device was operated with an X-ray sensor equipped with high efficiency XFlash 6 detectors (QUANTAX, Bruker Co., Billerica, Massachusetts, USA).

3.2.3. Contact angle

Contact angles have been measured by the sessile drop method with an FTA200 (First Ten Ångstroms Inc., Portsmouth, VA, USA) with some ad-hoc modifications. Three liquids have been used: water, diiodomethane and formamide. These pure liquids have relative permittivities: ε_W = 78.3, ε_{DIM} = 5.3 [27] and ε_{FA} = 108.2 [28]. Measurements have been performed at a 33 % relative humidity and 25ºC [29]. Because the inner membrane surfaces are cylinders, contact angles have been measured by considering such curvature. Final reported values are those extrapolated to zero volume sessile drop, obtained from measurements for increasing deposited volume of liquid. This procedure was intended to avoid any effect of the membrane curvature. Contact angle has been measured more than 5 times for each sample.

3.2.4. Measurements of Permeability

Permeability was measured with a tangential flow filtration apparatus provided with a cell for tubular membranes with controlled temperature, pressure and recirculation flow. The studied membranes had a length of 1200 mm but were cut in 231 mm segments to get them adapted to the membrane holder. The ends of the membrane segments were sealed giving an effective length of 221 mm and a filtration area of 4.863×10^{-3} m^2.

This filtration device was fed with deionized water at an average pressure (along the feed recirculation loop) of 6 bar and a recirculation flow of 1.5 L/min. Temperature went from 60 to 10 ºC in steps of about 10ºC. The standard deviation of temperature

was less than 1 ºC. The permeate flux was determined by weighting. The flow was considered stabilized when the permeated mass versus time gave a straight with correlations over 0.9999.

4. Results and Discussion

4.1. Atomic Force Microscopy (AFM)

In Fig. 3 the surfaces of the three membranes studied are shown with two different magnifications. It is easy to observe that the membranes In1nm and InLC have quite similar structures while In09nm is quite different with a rougher surface.

The root mean square (RMS) values for roughness, R_q, are shown in Fig. 4 where it appears clear that the In09nm membrane is substantially diferent to the other two membranes. An increase of roughness with increasing scanned areas is usual and correspond to a fractal like behavior [27]. The values shown in the figure are averages out of 5 measurements performed on different regions of the membrane surface. The In1nm and InLC membranes have almost constant and low roughness for scan sizes from 100nm to 1000nm. The corresponding fractal dimensions, as shown in the ***Supplementary Material,*** follow similar trends with more 2D behavior for both the In1nm and InLC membranes.

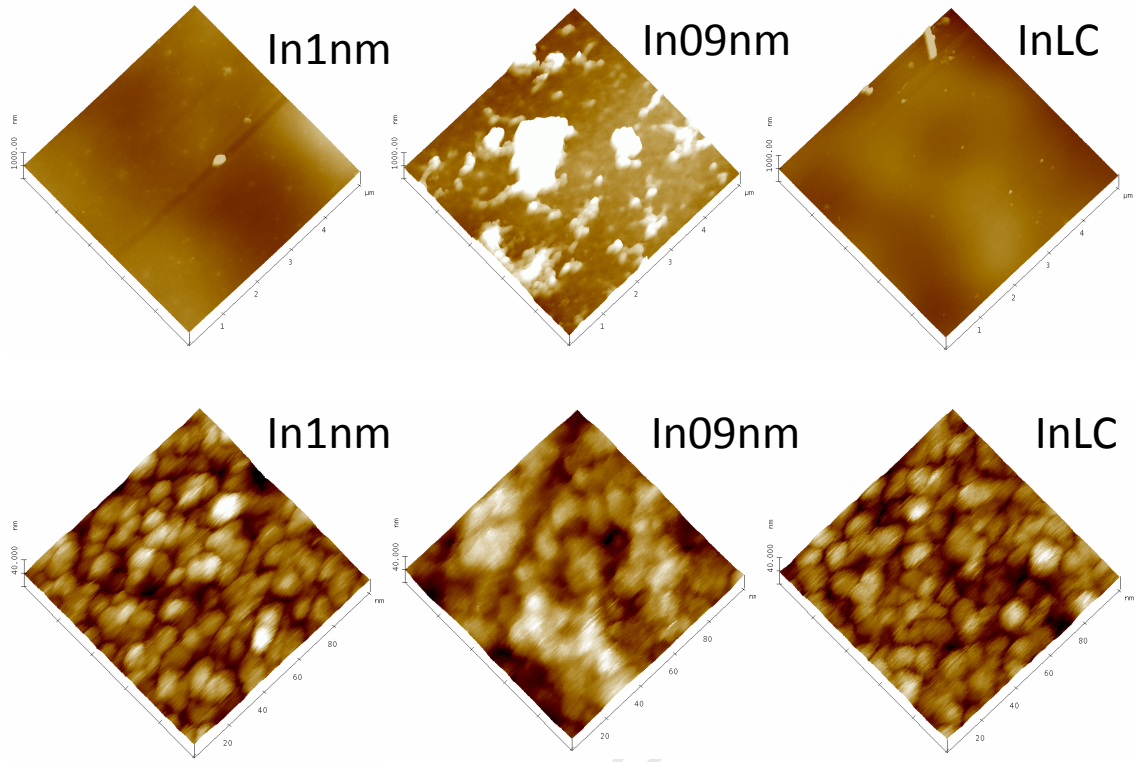

Fig. 3.- Topographic 5x5 µm images, top and 100x100 nm bottom for the tree membranes.

The 100 nm × 100 nm images in Fig. 3 show that all the membranes consist in elliptically shaped grains. Image analysis allows us to evaluate the grain size distribution on these AFM images. Fig. 5 shows the corresponding distribution for the In1nm membrane. In Table 2 the means and standard deviations for the grain size distributions for the three membranes studied are shown. These values correspond to the most probable ones for results obtained from 5 measurements on different areas of the membrane surface. It is clear, that also attending to grain size, as well as when considering roughness and fractal dimension, the In09nm is somehow different to the other two membranes.

Table 2: Parameters of the particle size distributions on the surfaces of the membranes studied as obtained from AFM image analysis.

Membrane	Mean grain size (nm)	Standard deviation (nm)
In1nm	8.6	2.7
In09nm	7.9	3.0
InLC	8.1	2.8

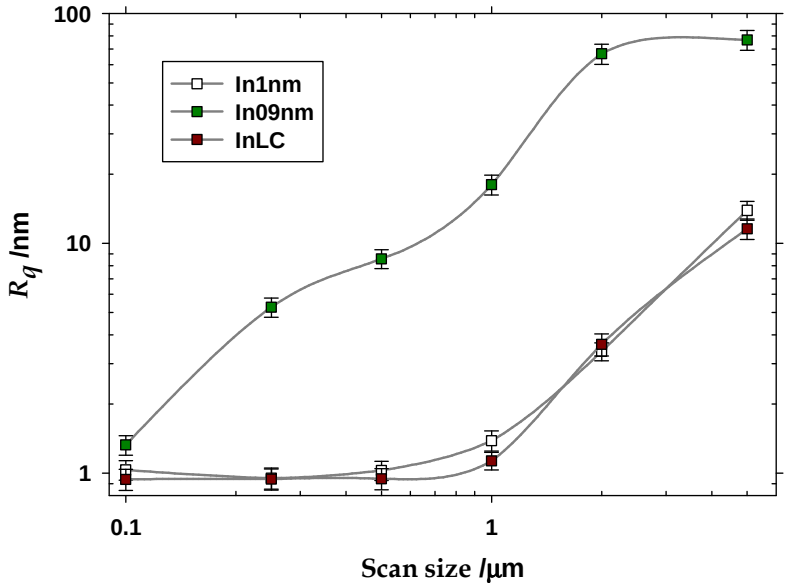

Fig. 4.- Roughness versus scan size for the three membranes studied.

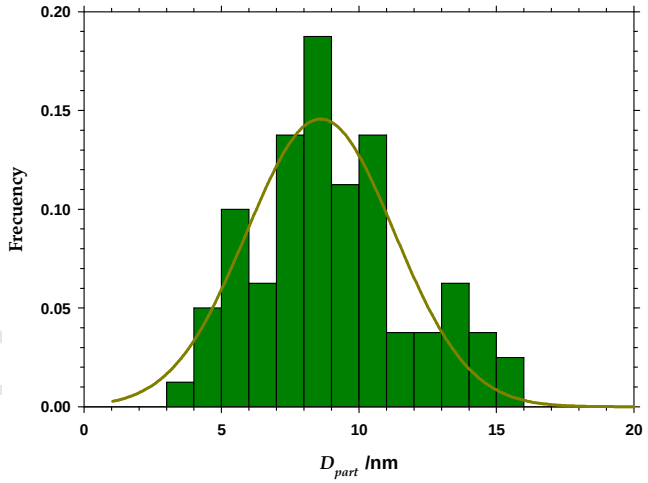

Fig. 5.-Grain size distribution for the In1nm membrane fitted to a Gaussian.

4.2. Scanning Electron Microscopy (SEM) and Energy Dispersive Spectroscopy (EDS)

The thickness of the studied membranes has been measured from SEM images of transversal sections. We have focused our attention on the titania active layers. An analysis of five points in five different micrographs allows us to get a significant statistics on the membrane thickness with the parameters shown in Table 3.

Table 3: Thickness and its standard deviation for the layers 2 and 3 (in Fig. 6). The layer 1 has a thickness of 18 μm [23].

Layer thickness	**2**	**3**
	Δx ± σ (nm)	
In1nm	805 ± 100	113 ± 12
In09nm	873 ± 46	206 ± 27 **(layer 3a in Fig. 6)** 84 ± 26 **(layer 3b in Fig. 6)**
InLC	702 ± 44	104.6 ± 5.6

In Fig. 6 several layers can be distinguished that are there labeled as 1, 2 and 3. All they are more easily identified in the BSE (Backscatter Electron Detector) images. In general the BSE images are more brilliant when they correspond to more dense materials [30]. First of all, there is a porous layer labeled 1 that, according to EDS, consists in Al_2O_3. The layer number 2 is mainly made of TiO_2, although some aluminum is also detected probably due to imprecise focusing of the electron beam that should detect the composition of layer 1 and 2 convoluted to some extent. Layer 3 is formed by two sub-layers for the In09nm but not for the other two membranes. These layers 3 are quite thin (from 0.05 to 0.2 μm) what causes imprecisions in the EDS results corresponding to them. In all cases there seems to be Zr in the layer 3 giving a quite brilliant image for this layer. In the case of the In09nm membrane, the active layer (3b) is less brilliant than the other sub-layer (3a) thus probably there is less Zr_2O in the active layer for this membrane. Results are compatible with an active layer (3b) consisting in TiO_2 or in TiO_2+ZrO_2 on a supporting sublayer (3a) made out of ZrO_2 or ZrO_2+TiO_2

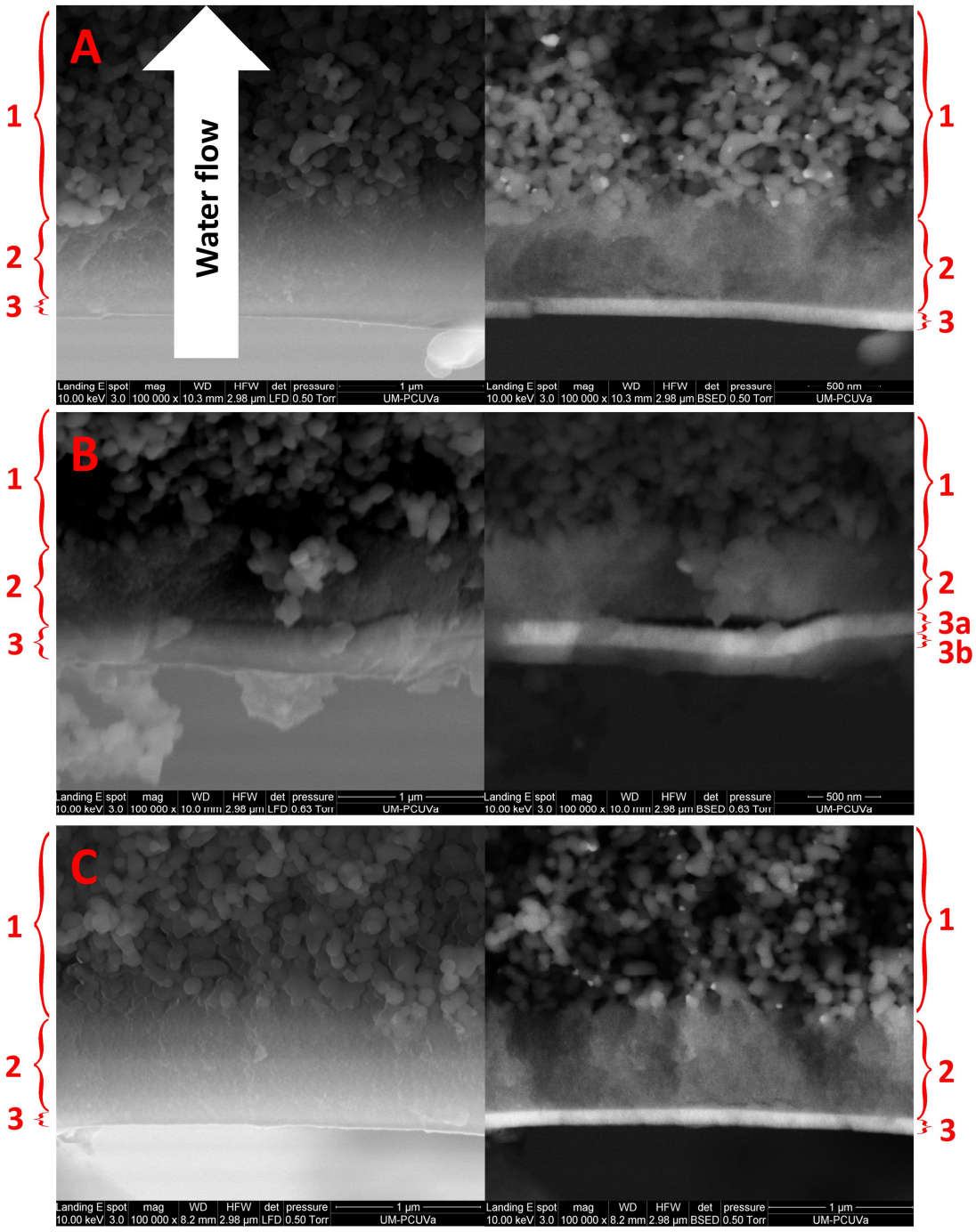

Fig. 6.- Scanning electron microscopy (SEM) micrographs of cross-section of In1nm (A), In09nm (B), and InLC (C). Left obtained from secondary electron detector (SED) and right obtained from backscatter electron detector (BSED). The arrow on the picture A indicates the flow from high to low pressure (from the active layer to the porous support). The same direction from the below upwards applies for the rest of the figures.

The EDS results on the active layer of the three membranes show that they contain TiO_2, ZrO_2 and Al_2O_3. In Table 4 the percentages of these oxides are shown for an acceleration voltage of 8kV (the corresponding spectra are shown in the ***Supplementary Material***). Due to the porous structure of the analyzed materials, the

beam could have penetrated to some extent to layer 2 and even to layer 1. Although these contributions might exist, they should be inversely proportional to the distance from the surface. An increase in the accelerating voltage would increase the penetration of the beam and actually reflects increasing contributions of TiO_2 and Al_2O_3 (se the corresponding table in the ***Supplementary Material***) probably because the electron beam reaches layers 2 and 1 more deeply. Finally, note that, also according to EDS results, once again, the In09nm membrane looks substantially different from the other two membranes studied.

Table 4: Percent composition of the three studied membranes according to EDS at 8 kV.

	TiO_2 %mol	**ZrO_2 %mol**	**Al_2O_3 %mol**
In1nm	54.2±2.7	36.1±1.8	09.7±0.5
In09nm	30.5±1.5	65.1±3.3	04.4±0.2
InLC	48.8±2.4	46.1±2.3	05.1±0.3

4.3. Contact Angle and Work of Adhesion

The contact angle results are shown in Table 5. The In09nm membrane seems to have higher affinity for water, and lower for diiodomethane, than the other membranes. Literature gives contact angles of 45º for flat TiO_2 membranes and 80º for ZrO_2 membranes [13]. Thus, our results appear compatible with membrane surfaces with TiO_2 and ZrO_2. with a higher proportion of TiO_2 for the In09nm membrane while the other two have higher proportions of ZrO_2, in accordance with the SEM and EDS results. Table 4 shows that the In09nm membrane appears to contain less TiO_2 and should give the highest contact angle. Nevertheless, if we take into account that Zr produces most backscattered electrons, the image in Figure 6-B left shows that the 3b layer (which is the actual interface with the retentate side) contains less Zr and consequently more TiO_2 than the layer immediately below it (layer 3a). This would justify that the contact angle for the In09nm membrane would be determined by this high content of TiO_2. It is worth noting that element percentages in Table 4 correspond to the signal detected after normal incidence thus penetrating to layers 3a and 2.

Attending to the evaluated work of adhesion for water it is clear that in effect the In09nm membrane is more hydrophilic than the other two membranes. From the contact angles for the three liquids consigned in Table 5 we can evaluate the surface tension of the solid for the three membranes, γ_{solid}, which actually gives quite similar

values. But the In09nm membrane seems to be more polar, γ_{solid}^{polar}, than the other two membranes that, in turn, give higher contribution of dispersive interactions, $\gamma_{solid}^{dispersive}$, on the surface tension [29]. In the ***Supplementary Material***, the equations used to get the parameters shown in Table 5 are shown.

Table 5: Contact angles and work of adhesion of water and components of surface tension.

	Contact Angle, θ^0			$W_{adhesion\ of\ water}$	$\gamma_{solid}^{dispersive}$	γ_{solid}^{polar}	γ_{solid}
	Water H_2O	**Diiodomethane CH_2I_2**	**Formamide $HCONH_2$**	**(mJ/m2)**	**(mJ/ m^2)**	**(mJ/ m^2)**	**(mJ/ m^2)**
In1nm	66.5±1.4	29.5±0.9	34.5±1.0	101.8±1.9	44.4±0.8	7.7±0.3	52.08±0.8
In09nm	63.7±1.3	41.2±1.0	34.9±1.1	105.1±2.0	39.0±0.7	10.7±0.4	49.74±0.8
InLC	67.2±1.5	37.4±0.9	35.1±0.9	101.0±1.9	40.9±0.8	8.2±0.4	49.09±0.7

4.4. Water Permeability

In Fig. 7 the water permeability, $L_p = J_V/\Delta p$, as a function of temperature is shown for the three membranes studied. Fig. 7 shows that there is not any correlation of L_p with the molecular weight cut-off (MWCO) (see Table 1). Actually, for example, the In09nm membrane gives the lowest L_p in spite of having intermediate MWCO. Because it seems reasonable to assume a negligible change in the porous structure of the membranes in the range of temperatures studied, we can attribute the increase of permeability to changes in the viscosity of water.

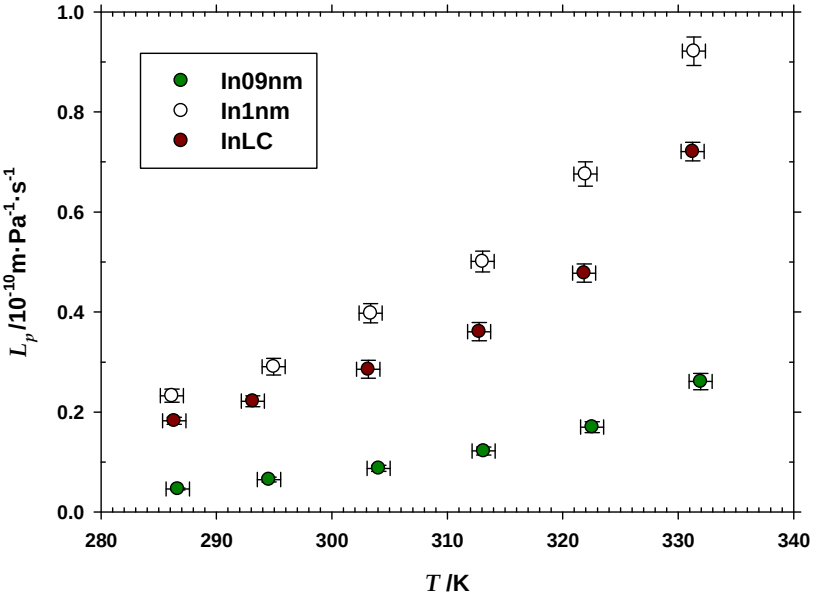

Fig. 7- Permeability versus temperature for the membranes studied.

4.5. Analysis of the Models Proposed here

The evaluation of the Darcy's constant (Eq. (1)) requires the multiplication of the permeability by the thickness of the active layer (assuming, as usually done, that the pressure drop along the Support layer is negligible), $K = L_p l_m$. For these thickness we will take here those for the layer 3 for the In01nm and InLC membranes and for the 3b layer for the In09nm membrane (see Table 3). For the pore radii we will take the nominal values given by the manufacturers for two of the membranes and the MWCO for all the studied membranes. We will get the effective mean pore radii from a correlation proposed by Van der Bruggen and C.Vandecasteele obtained from experimental results on retention of PEGs through NF membranes [31]:

$$r_p = 0.0325 MW^{0.438} \quad (23)$$

Here MW stands for the MWCO in Da as shown in Table 1 and r_p in nm. This equation gives pore radii of 0.59, 0.47 and 0.33 nm, for the membranes In1nm, In0.9nm and InLC. These values reasonably agree with the values (diameters) given by the manufacturer in Table 1.

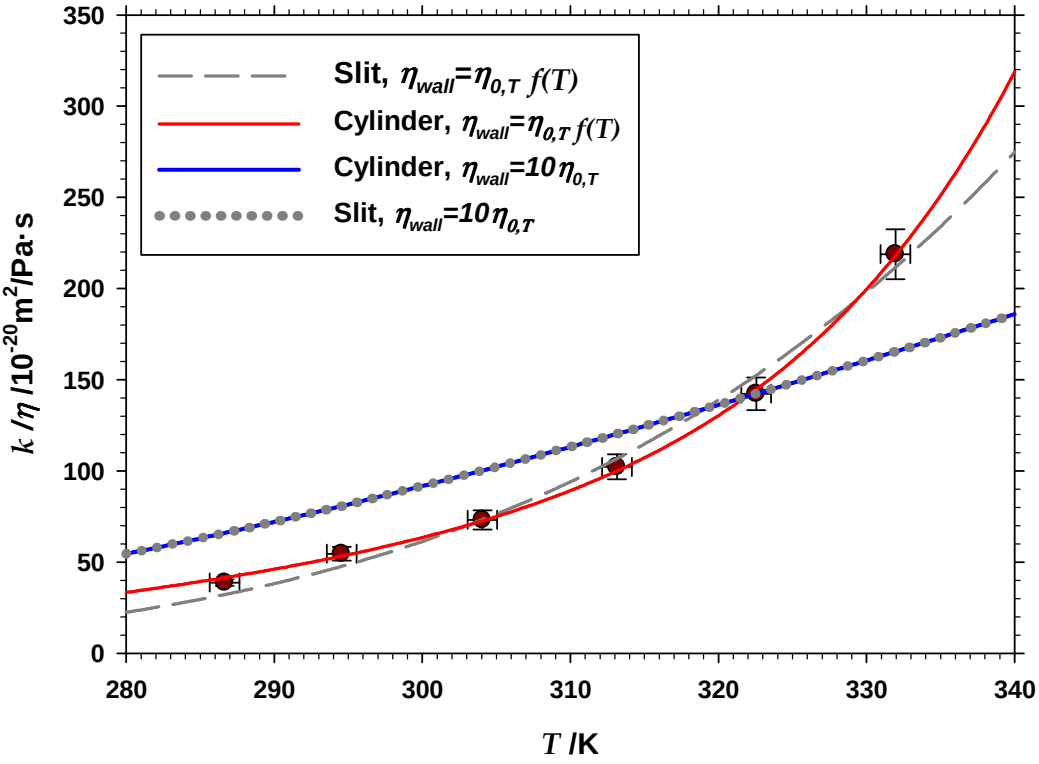

Fig. 8.- Darcy's constant in function of temperature for the In09nm membrane. Symbols correspond to the experimental results while lines follow the different models studied and identified on the figure.

The Darcy's constant (according to $k/\eta = K = J_V\left(l_m/\Delta p\right) = L_p l_m$) as a function of temperature and the corresponding fitting of the models are shown in Fig. 8 for the In09nm membrane (the other two membranes give very similar behaviors as shown in the Supplementary Material). Fittings have been performed by using a Marquardt Levenberg algorithm. Only the models that consider viscosity on the wall, η_{wall}, as depending on temperature in an Arrhenius mode (Eqs. (20) and (21)) pass the normality Shapiro-Wilk test. It appears clearly that the assumption of a layer in contact with the pore walls with a viscosity 10 times that of the bulk water is totally inadequate. On the contrary, the models that assume an Arrhenius process of adsorption are much better fitted. In particular, in our case, the pores seem to be cylindrical. The slit shaped pore model gave $r^2 > 0.970$ while for cylindrical pores $r^2 > 0.999$. In Table 6 the corresponding fitted parameters for the three membranes are shown for the cylindrical pores. Of course, the goodness of the respective fittings is not a strong enough reason to discriminate between cylindrical and slit-shaped pores. Nevertheless, if we add to this the fact that AFM shows an agglomeration of almost spherical particles and that an

assumption of slit-shaped pores would give activation energies from -1.3 to -2 kJ/mol that are far from those typical of TiO2 or ZrO2 [32, 33], we can opt for cylindrical pores.

Table 6: Fitted parameters of Eq. (21) (cylindrical pores).

	$k(10^{-20}m^2)$	A(dimensionless)	$E_a(kJ/mol)$
In1nm	3.9±0.2	(1.8±0.7)×10^{-6}	-44±9
In09nm	1.68±0.12	(3.2±0.9)×10^{-7}	-51±6
InLC	21.11±0.11	(1.8±0.9)×10^{-13}	-95±3

The activation energy for water adsorption, E_a, is negative which means that the three membranes are hydrophilic. The frequency factor A gives an idea of the mobility of the adsorbed molecules of water that appear to decrease with decreasing pore sizes as seems reasonable. E_a increases for smaller pore sizes what means that confinement can increase the water-wall interactions increasing hydrophilicity. If confinement was irrelevant, the In09nm membrane should give the highest E_a in accordance with its highest adhesion work (see Table 5). The effect of confinement on the interaction energy has been studied by other authors showing that in TiO2 nanopores a decrease of the surface curvature radius (narrower pores) produces an increase of E_a and hydrophilicity [14, 34]. In fact, the value of E_a could be too high to be attributed only to a high confinement [35]. It is worth noting that we deal with a fitting procedures to get three parameters, two of them (A and E_a) exponentially linked. Obtaining more reliable values for E_a would require more specific techniques as NMR Relaxometry, for example. This technique would lead to additional evidences to decide between cylindrical and slit-shaped pores by an analysis of mono-dimensional versus bi-dimensional diffusion [32].

It seems clear that the surface structure of our membranes was granular with grain sizes as shown in Table 2, thus the Carman-Kozeny equation should be applicable. If we assume k as given by each model (Eqs. (13), (14), (21) and (22)) for the viscosity in the nanopores and we use Eq. (10), we could compare the predicted grain size with

the experimental one measured by AFM. In order to be able to perform this, we would need porosity (see Eq. (10)). The manufacturers give porosities in the range from 30 to 40 (see Table 1). A more precise porosity ($\varepsilon = 30\%$) can be found in the literature for the In09nm membrane [26]. We will use this porosity for the In09nm membrane. In Table 7, the corresponding grain sizes evaluated in this way are shown along with the corresponding percentage of deviation when compared with the AFM grain sizes (see Table 2).

Table 7: Diameter of the particles forming the membrane obtained from the Carman-Kozeny equation (Eq. (10)) for the k fitted from the different models applied to the membrane In09nm. The percentages of deviation from the particle size as measured by AFM are also shown.

Model	$D_{part}(nm)$	$\frac{D_{part}-D_{part,AFM}}{D_{part,AFM}}100 \quad (\%)$
Slit $\eta_{wall}=10\eta_{0,T}$	3.99 ± 0.18	-49.2
Cylinder $\eta_{wall}=10\eta_{0,T}$	4.53 ± 0.2	-42.4
Slit $\eta_{wall}=\eta_{0,T}f(T)$	10.24 ± 0.01	+30.2
Cylinder $\eta_{wall}=\eta_{0,T}f(T)$	7.42 ± 0.2	-5.7

The model of cylindrical pores with a viscosity on the pore walls correlated with temperature by an Arrhenius dependence (Eq. (22)) gives grain sizes that are nearly only 6 % different of those measured by AFM. If alternatively, we accept the Carman-Kozeny equation we can calculate porosities from the grain sizes measured by AFM. The resulting porosities are shown in Table 8.

Table 8: Porosity evaluated by Eq. (10).

	$\varepsilon(\%)$
In1nm	34±5
In09nm	29±2
InLC	51±8

The porosity of both In1nm and In09nm membranes are within the nominal range given by the manufacturer. Fort the InLc membrane we get a high porosity which is over that given by the manufacturer. Nevertheless, the specifications given by the manufacturer consist in a common range for the three membranes, without any information on the technique used.

In any case, the agreement of porosities or grain sizes is quite significant and corroborates that the assumptions of cylindrical pores with viscosities on the pore walls determined by an Arrhenius law are adequate.

5. Conclusions

We used three inorganic ceramic nanofiltration membranes to study the flow of pure water as a function of temperature, to get information on the water viscosity in confined pores within the nanometric range. We have shown that the usual models, that assume that the ratio of the viscosity of water on the pore walls over that in bulk water is a constant, are totally inadequate to predict the Darcy constant versus temperature behavior.

Structural parameters of the studied membranes (grain size and thickness of the layers within the membranes have been determined by AFM and SEM. Results show that the three membranes have active layers around 100 nm in thickness consisting in more or less spherical particles of about 8 nm. Hydrophilicity and chemical nature of the active layer was studied by EDS and contact angles to reveal that the three membranes have very similar chemistry and hydrophilic character although both these aspects are clearly correlated.

Water flux as a function of temperature, although not concluding, give some evidence in favor of a cylindrical pore model with a monomolecular adsorbed layer with a viscosity over the bulk (unconfined) one. In all cases it has been found that by assuming that the first layer of water on the pore walls moves with a viscosity $\eta_{wall} = f(T)\eta_0$ with $f(T) = Ae^{-\frac{E_a}{RT}}$, a fine concordance with the experimental values of the Darcy constant is obtained.

If now we assume the Carman-Kozeny equation corresponding to granular materials and pores left by their interstices we get a fair agreement (deviation below 5 %) between the AFM measured grain sizes for the active layer of the three membranes studied and those predicted by the Carman-Kozeny equation with our η_{wall} model.

In summary, we have shown that for membranes consisting in nanometric cylindrical pores assimilated to the actual paths left by the interstices within the granular structure, as those analyzed here, we can assume that there is a layer of water on the pore walls with a viscosity bigger than the bulk (unconfined) viscosity. The proportionality constant depends on temperature by an Arrhenius type correlation. This is a valuable contribution to the study of the complex convolution of size, electrical and dielectric factors that should enter any useful model to explain nanofiltration flux and retention.

6. Symbol lists

A	Frequency factor in Arrhenius equation (dimensionless)
A_m	Membrane area (m^2)
A_ε	Membrane area opened to flow (m^2)
D_{part}	Average particle diameter (m)
d	Size of the first adsorbed water layer (m)
E_a	Activation energy for water adsorption (J/mol)
f_C	Water and membrane interaction function (dimensionless)
h	Size of slit-like pores (m)
J_V	Permeate volume flow per unit of area (m/s)
$J_{V,HP}$	Hagen-Poiseuille Permeate volume flow per unit of area (m/s)
K	Darcy's constant ($m^3 \cdot s/kg$)
k	Darcy's constant multiplied by viscosity (m^2)
L_p	Water permeability ($m/s \cdot Pa$)
l	Pores length (m)
l_m	Thickness of the membrane (m)
MW	Molecular weight (g/mol)
n_p	Number of pores per unit of area (m^{-2})
Q_V	Permeate volume flow (m^3/s)
R	Gas constant (J/K·mol)
R_q	Root mean square of the roughness (m)
r	Radial coordinate (m)
r_p	Pore radius (m)

$r_{p,slit}$	Equivalent radius of slit-like pores (m)
T	Temperature (K)
v	Tangential speed inside of pore (m/s)
$W_{adhesion\ of\ water}$	Water adhesion work (J/m^2)

Greeks letters

γ_{solid}	Surface tension of the solid (J/m^2)
$\gamma_{solid}^{dispersive}$	Dispersive contribution of the surface tension of the solid (J/m^2)
γ_{solid}^{polar}	Polar contribution of the surface tension of the solid (J/m^2)
Δp	Pressure drop (Pa),
δ	Slipping length (m)
ε	Porosity (%)
ε_{DIM}	Relative permittivity of diiodomethane (dimensionless)
ε_{FA}	Relative permittivity of formamide (dimensionless)
ε_{W}	Relative permittivity of water (dimensionless)
φ	Function of d/r_p in Eq. (17) (1/ Pa·s)
η	Viscosity (Pa·s)
η_p	Viscosity inside the pores (Pa·s)
$\eta_{p,slit}$	Viscosity inside of slit-like pores (Pa·s)
η_0	Bulk viscosity (Pa·s)
$\eta_{0,T}$	Bulk viscosity as a function of temperature (Pa·s)
η_{wall}	Viscosity of water on the pore walls (Pa·s)
θ	Contact angle (dimensionless)
τ	Tortuosity factor (dimensionless)

7. Acknowledgements

Authors would like to thank the Spanish Government for its fainancement through project MAT2016-76413-C2-1-R and to the Regional Government of Castilla y León and the EU-FEDER programme (CLU2017-09, UIC082, VA088G19).

8. References

[1] A.W. Mohammad, Y.H. Teow, W.L. Ang, Y.T. Chung, D.L. Oatley-Radcliffe, N. Hilal, Nanofiltration membranes review: Recent advances and future prospects, Desalination, 356 (2015) 226-254.

[2] W.R. Bowen, J.S. Welfoot, Modelling the performance of membrane nanofiltration—critical assessment and model development, Chemical Engineering Science, 57 (2002) 1121-1137.

[3] V. Silva, V. Geraldes, A.M.B. Alves, L. Palacio, P. Pradanos, A. Hernandez, Multi-ionic nanofiltration of highly concentrated salt mixtures in the seawater range, Desalination, 277 (2011) 29-39.
[4] V. Silva, M. Montalvillo, F. Javier Carmona, L. Palacio, A. Hernandez, P. Pradanos, Prediction of single salt rejection in nanofiltration membranes by independent measurements, Desalination, 382 (2016) 1-12.
[5] F. Durst, Fluid Mechanics. An Introduction to the Theory of Fluid Flows, Springer, Berlin, 2008.
[6] S. Middleman, An Introduction to Fluid Dynamics, John Wiley, New York, 1998.
[7] K. Wesolowska, S. Koter, M. Bodzek, Modelling of nanofiltration in softening water, Desalination, 162 (2004) 137-151.
[8] M. Montalvillo, V. Silva, L. Palacio, J.I. Calvo, F.J. Carmona, A. Hernández, P. Prádanos, Charge and dielectric characterization of nanofiltration membranes by impedance spectroscopy, Journal of Membrane Science, 454 (2014) 163-173.
[9] G. Hu, D. Li, Multiscale phenomena in microfluidics and nanofluidics, Chemical Engineering Science, 62 (2007) 3443-3454.
[10] P. Abgrall, N.T. Nguyen, Nanofluidic Devices and Their Applications, Analytical Chemistry, 80 (2008) 2326-2341.
[11] S.K. Kannam, B.D. Todd, J.S. Hansen, P.J. Daivis, Slip length of water on graphene: Limitations of non-equilibrium molecular dynamics simulations, The Journal of Chemical Physics, 136 (2012) 024705.
[12] V.P. Sokhan, D. Nicholson, N. Quirke, Fluid flow in nanopores: An examination of hydrodynamic boundary conditions, The Journal of Chemical Physics, 115 (2001) 3878-3887.
[13] P. Marchetti, A. Butté, A.G. Livingston, An improved phenomenological model for prediction of solvent permeation through ceramic NF and UF membranes, Journal of Membrane Science, 415-416 (2012) 444-458.
[14] E. González Solveyra, E. de la Llave, V. Molinero, G.J.A.A. Soler-Illia, D.A. Scherlis, Structure, Dynamics, and Phase Behavior of Water in TiO2 Nanopores, The Journal of Physical Chemistry C, 117 (2013) 3330-3342.
[15] M.I. Velasco, M.B. Franzoni, E.A. Franceschini, E. Gonzalez Solveyra, D. Scherlis, R.H. Acosta, G.J.A.A. Soler-Illia, Water Confined in Mesoporous TiO2 Aerosols: Insights from NMR Experiments and Molecular Dynamics Simulations, The Journal of Physical Chemistry C, 121 (2017) 7533-7541.
[16] J. Bear, Dynamics of Fluids in Porous Media, Dover, New York, 1972.
[17] P. Pradanos, J.I. Arribas, A. Hernandez, Hydraulic Permeability, Mass Transfer, and Retention of PEGs in Cross-flow Ultrafiltration through a Symmetric Microporous Membrane, Separation Science and Technology, 27 (1992) 2121-2142.
[18] R.C. Kuhn, F. Maugeri Filho, V. Silva, L. Palacio, A. Hernandez, P. Pradanos, Mass transfer and transport during purification of fructooligosaccharides by nanofiltration, Journal of Membrane Science, 365 (2010) 356-365.
[19] V.G. Levich, Physicochemical Hydrodynamics, Prentice-Hall, Inc., Englewook Cliffs, New Jersey, 1962.
[20] L. Bocquet, J.-L. Barrat, Hydrodynamic boundary conditions, correlation functions, and Kubo relations for confined fluids, Physical Review E, 49 (1994) 3079-3092.
[21] D.I. Dimitrov, A. Milchev, K. Binder, Forced imbibition—a tool for separate determination of Laplace pressure and drag force in capillary filling experiments, Physical Chemistry Chemical Physics, 10 (2008) 1867-1869.
[22] J.N. Israelachvili, Intermolecular and Surface Forces, Academic Press, Amsterdam, 2011.
[23] R. Shang, A. Goulas, C.Y. Tang, X. de Frias Serra, L.C. Rietveld, S.G.J. Heijman, Atmospheric pressure atomic layer deposition for tight ceramic nanofiltration membranes: Synthesis and application in water purification, Journal of Membrane Science, 528 (2017) 163-170.

[24] R. Metzler, R.P. Rauschert, V. Prehn, Chemical and mechanical resistance, Inopor Report, Inopor GmbH, Veilsdorf, Germany, 2008.
[25] R. Metzler, R.P. Rauschert, V. Prehn, Geometries, materials and pore sizes, Inoport Report, Inopor GmbH, Germany, 2015.
[26] I. Voigt, S.T. Wöhner, M. Stahn, M. Schleifenhemer, A. Junghans, J. Rost, Bewährungsprobe bestanden. Neu entwickelte keramische NF-membran im praxiseinsatz, Verfahrenstechnik, 36 (2002) 17-19.
[27] J.E. Rumble, Handbook of Chemistry and Physics, 99th ed., CRC Press, Boulder, 2018.
[28] V.P. Pawar, S.C. Mehrotra, Dielectric relaxation study of chlorobenzene with formamide at microwave frequency using time domain reflectometry, Journal of Molecular Liquids, 115 (2004) 17-22.
[29] L. Fernandez, M. Sanchez, F.J. Carmona, L. Palacio, J.I. Calvo, A. Hernandez, P. Pradanos, Analysis of the Grafting Process of PVP on a Silicon Surface by AFM and Contact Angle, Langmuir, 27 (2011) 11636-11649.
[30] T. Van Gestel, D. Sebold, W.A. Meulenberg, M. Bram, H.-P. Buchkremer, Manufacturing of new nano-structured ceramic–metallic composite microporous membranes consisting of ZrO2, Al2O3, TiO2 and stainless steel, Solid State Ionics, 179 (2008) 1360-1366.
[31] B. Van der Bruggen, C. Vandecasteele, Modelling of the retention of uncharged molecules with nanofiltration, Water Research, 36 (2002) 1360-1368.
[32] F. Parrino, P. Conte, C. De Pasquale, V.A. Laudicina, V. Loddo, L. Palmisano, Influence of Adsorbed Water on the Activation Energy of Model Photocatalytic Reactions, The Journal of Physical Chemistry C, 121 (2017) 2258-2267.
[33] P. Raghu, C. Yim, F. Shadman, E. Shero, Susceptibility of SiO2, ZrO2, and HfO2 dielectrics to moisture contamination, AIChE Journal, 50 (2004) 1881-1888.
[34] S. Kenmoe, O. Lisovski, S. Piskunov, D. Bocharov, Y.F. Zhukovskii, E. Spohr, Water Adsorption on Clean and Defective Anatase TiO2 (001) Nanotube Surfaces: A Surface Science Approach, The Journal of Physical Chemistry B, 122 (2018) 5432-5440.
[35] E.A. Krylova, M.G. Shelyapina, P. Nowak, H. Harańczyk, M. Chislov, I.A. Zvereva, A.F. Privalov, M. Becher, M. Vogel, V. Petranovskii, Mobility of water molecules in sodium- and copper-exchanged mordenites: Thermal analysis and 1H NMR study, Microporous and Mesoporous Materials, 265 (2018) 132-142.

Highlights

- Water permeability through ceramic nanofiltration membranes is studied.
- A model for water viscosity inside nanopores is proposed.
- The changes in viscosity with temperature are studied.
- The Carman-Kozeny model and our water viscosity model agree with the membrane granular morphology.

Declaration of interests

■ The authors declare that they have no known competing financial interests or personal relationships that could have appeared to influence the work reported in this paper.

☐The authors declare the following financial interests/personal relationships which may be considered as potential competing interests: